Surface-emitting circular DFB, disk-, and ring-Bragg resonator lasers with chirped gratings. II: nonuniform pumping and far-field patterns

Xiankai Sun[*] and Amnon Yariv

Department of Applied Physics, MC128-95, California Institute of Technology, Pasadena, CA 91125, USA
[*]Corresponding author: xksun@caltech.edu

Abstract: This is a continuation of our previous work [Opt. Express **16,** 9155 (2008)]. In this paper we investigate the effect of nonuniform pumping on the modal properties of surface-emitting chirped circular grating lasers. By numerically solving the coupled-mode equations and matching the boundaries we compare and discuss the threshold pump levels and frequency detuning factors for three pumping profiles: uniform, Gaussian, and annular. Depending on the overlap of the pumping and modal profiles, Gaussian pumping results in the lowest threshold pump levels except for the fundamental mode of ring Bragg resonator laser, and annular pumping provides larger threshold discrimination between the fundamental and first-order modes of circular DFB and ring Bragg resonator lasers, which is favorable for single-mode operation in these lasers. We also study the far-field patterns of the fundamental modes of circular DFB, disk-, and ring-Bragg resonator lasers. Circular DFB and ring Bragg resonator lasers have the first-order dominating peak, while disk Bragg resonator laser exhibits the zeroth-order dominating peak.

OCIS codes: (250.7270) Vertical emitting lasers; (140.5560) Pumping; (130.2790) Guided waves; (230.1480) Bragg reflectors; (050.2770) Gratings; (140.5960) Semiconductor lasers; (130.0130) Integrated optics.

References and links

1. J. Scheuer and A. Yariv, "Coupled-Waves Approach to the Design and Analysis of Bragg and Photonic Crystal Annular Resonators," IEEE J. Quantum Electron. **39**, 1555-1562 (2003).
2. J. Scheuer and A. Yariv, "Annular Bragg defect mode resonators," J. Opt. Soc. Am. B **20**, 2285-2291 (2003).
3. X. K. Sun and A. Yariv, "Surface-emitting circular DFB, disk-, and ring- Bragg resonator lasers with chirped gratings: a unified theory and comparative study," Opt. Express **16**, 9155-9164 (2008).
4. C. Olson, P. L. Greene, G. W. Wicks, D. G. Hall, and S. Rishton, "High-order azimuthal spatial modes of concentric-circle-grating surface-emitting semiconductor lasers," Appl. Phys. Lett. **72**, 1284-1286 (1998).
5. J. Scheuer, W. M. J. Green, G. A. DeRose, and A. Yariv, "InGaAsP Annular Bragg Lasers: Theory, Applications, and Modal Properties," IEEE J. Sel. Top. Quantum Electron. **11**, 476-484 (2005).
6. C. Wu, T. Makino, M. Fallahi, R. G. A. Craig, G. Knight, I. Templeton, and C. Blaauw, "Novel Circular Grating Surface-Emitting Lasers with Emission from Center," Jpn. J. Appl. Phys. **33-Pt. 2**, L427-L429 (1994).
7. K. J. Kasunic, E. M. Wright, and N. Peyghambarian, "Numerical modeling of inhomogeneously-pumped circular-grating DFB lasers," Proc. SPIE **2398**, 125-134 (1995).
8. P. L. Greene and D. G. Hall, "Effects of Radiation on Circular-Grating DFB Lasers—Part II: Device and Pump-Beam Parameters," IEEE J. Quantum Electron. **37**, 364-371 (2001).
9. G. A. Turnbull, A. Carleton, A. Tahraouhi, T. F. Krauss, I. D. W. Samuel, G. F. Barlow, and K. A. Shore, "Effect of gain localization in circular-grating distributed feedback lasers," Appl. Phys. Lett. **87**, 201101 (2005).
10. A. M. Shams-Zadeh-Amiri, X. Li, and W.-P. Huang, "Above-Threshold Analysis of Second-Order Circular-Grating DFB Lasers," IEEE J. Quantum Electron. **36**, 259-267 (2000).
11. G. F. Barlow, A. Shore, G. A. Turnbull, and I. D. W. Samuel, "Design and analysis of a low-threshold polymer circular-grating distributed-feedback laser," J. Opt. Soc. Am. B **21**, 2142-2150 (2004).

#103822 - $15.00 USD Received 7 Nov 2008; revised 18 Dec 2008; accepted 18 Dec 2008; published 22 Dec 2008

12. X. K. Sun, J. Scheuer, and A. Yariv, "Optimal design and reduced threshold in vertically emitting circular Bragg disk resonator lasers," IEEE J. Sel. Top. Quantum Electron. **13**, 359-366 (2007).
13. X. K. Sun and A. Yariv, "Modal properties and modal control in vertically emitting annular Bragg lasers," Opt. Express **15**, 17323-17333 (2007).
14. A. Yariv, *Quantum Electronics*, 3rd ed. (Wiley, New York, 1989).
15. E. Hecht, *Optics*, 3rd ed. (Addison-Wesley, 1998).
16. R. H. Jordan, D. G. Hall, O. King, G. Wicks, and S. Rishton, "Lasing behavior of circular grating surface-emitting semiconductor lasers," J. Opt. Soc. Am. B **14**, 449-453 (1997).
17. M. Fallahi, M. Dion, F. Chatenoud, I. M. Templeton, R. Barber, and J. Sedivy, "Low Threshold CW Operation of Circular-Grating Surface-Emitting DBR Lasers Using MQW and a Self-Aligned Process," IEEE Photon. Technol. Lett. **6**, 1280-1282 (1994).

1. Introduction

Circular grating coupled surface emitting lasers are able to produce circularly-symmetric, large-emission-aperture, narrow-divergence laser beams, which makes them not only excellent light emitters with efficient coupling to optical fibers but also superior elements for on-chip 2D laser array integration for coherent beam combination. As shown in Fig. 1, three configurations of such circular grating lasers have been extensively investigated: (a) Circular DFB lasers, in which the grating extends from the center to the exterior boundary x_b. (b) Disk Bragg resonator lasers, in which a center disk is surrounded by a radial Bragg grating extending from x_0 to x_b. (c) Ring Bragg resonator lasers, in which an annular defect is surrounded by inner and outer gratings on both sides. The inner grating extends from the center to x_L while the outer from x_R to x_b. In these lasers, the gratings serve two purposes − providing feedback for the in-plane fields to form a radial resonator, and coupling the vertical laser radiation out of the plane as an output coupler. Detailed in [1] and [2], the gratings have to be designed *radially chirped* in order to optimally interact with the optical fields since the eigenmodes of the wave equation in cylindrical coordinates, the Bessel functions, have nonperiodic zeros.

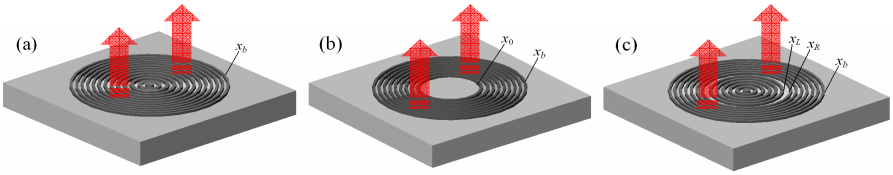

Fig. 1. Surface-emitting chirped circular grating lasers: (a) Circular DFB laser; (b) Disk Bragg resonator laser; (c) Ring Bragg resonator laser. Laser radiation is coupled out of the resonators in vertical direction via the gratings.

In Part I of this series of papers [3], we developed a unified theory for solving and comparing modal properties of the aforementioned types of surface-emitting chirped circular grating lasers. A comparative study concluded that disk Bragg resonator lasers are most useful in low-threshold, high-efficiency, ultracompact laser design, while ring Bragg resonator lasers are excellent candidates for high-efficiency, high-power, large-area lasers. These results clearly demonstrate the advantages of disk and ring types Bragg resonator lasers and point out their potential applications. For the purpose of analytical derivations, a uniform pumping profile – thus a uniform gain distribution – was assumed in the model. However, in practical experimental situations, the pumping profile is usually nonuniform, distributed either in a Gaussian shape in optical pumping [4, 5] or in an annular shape in electrical pumping [6]. The effects of nonuniform pumping profiles [7-9] and modal far-field patterns [10, 11] were studied previously only for circular DFB lasers. In this paper by solving the coupled-mode equations and matching boundaries in a numerical way we present a comprehensive study of the nonuniform pumping, especially the effects on the threshold pump levels and frequency detuning factors, for those three types of circular grating lasers. Then their far-field patterns will be calculated, compared, and discussed, which is followed by the conclusions.

#103822 - $15.00 USD Received 7 Nov 2008; revised 18 Dec 2008; accepted 18 Dec 2008; published 22 Dec 2008

2. Coupled-mode equations, boundary conditions, and numerical methods

The coupled-mode equations for the Hankel-phased circular gratings in active media were derived in [12] and [13] including the effect of resonant vertical radiation. By using the Green's function method, the contribution from vertical radiation is incorporated as a coefficient into the coupled in-plane wave equations, yielding a set of evolution equations for the amplitudes of the in-plane waves

$$\begin{cases} \dfrac{dA(x)}{dx} = u(x)\cdot A(x) - v\cdot B(x)\cdot e^{2i\delta\cdot x} \\ \dfrac{dB(x)}{dx} = -u(x)\cdot B(x) + v\cdot A(x)\cdot e^{-2i\delta\cdot x}. \end{cases} \tag{1}$$

In the above equations, A and B denote the amplitudes of the in-plane outgoing and incoming propagating cylindrical waves, respectively. The normalized radius x is defined as $x=\beta\rho$. The normalized frequency detuning factor $\delta=(\beta_{design}-\beta)/\beta$ represents the relative frequency shift from the optimal coupling design. The coefficients u and v are defined as $u(x)=g(x)-h_1$, $v=h_1+ih_2$, where $g(x)$ is the position-dependent net gain coefficient the shape of which follows that of the pumping profile. h_1 and h_2 are, respectively, the radiation- and feedback- coupling coefficients, the calculation of which involves the Fourier expansion coefficients of the grating profile. For no-grating regions, e.g., the center disk in disk Bragg resonator laser and the annular defect in ring Bragg resonator laser, h_1 and h_2 vanish. It should be noted that Eqs. (1) implicitly include the effect of vertical radiation via h_1, which is treated as a loss term in obtaining the modal threshold levels.

All the circular grating lasers including the three configurations shown in Fig. 1 have to satisfy the common boundary conditions: (i) $A(0)=B(0)$ at the center; (ii) $B(x_b)=0$ at the exterior boundary x_b; (iii) $A(x)$ and $B(x)$ are continuous for all $0<x<x_b$. As already discussed in [3], boundary condition (iii) is equivalent to the continuities of both the in-plane electric field and its first derivative.

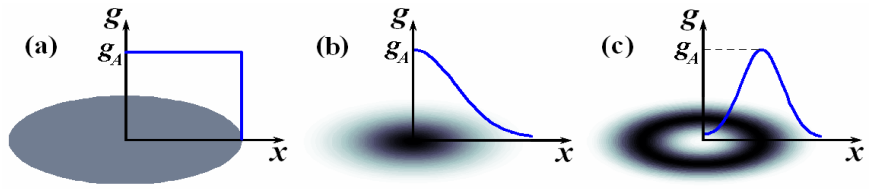

Fig. 2. Illustration of different gain distribution profiles: (a) uniform; (b) Gaussian; (c) annular.

For a certain gain distribution profile, $g(x)$ is parameterized with a proportion constant, say, its maximal value g_A. To numerically solve Eqs. (1), we start with the amplitude set $[A\ B] = [1\ 1]$ at the center, then integrate the coupled equations to the exterior boundary x_b. The absolute value of $B(x_b)$ marks a contour map in the 2-D plane of g_A and δ. Identifying each minimum point in the contour map gives us the threshold g_A and the detuning factor δ pertaining to a mode. However, the parameter g_A can be arbitrarily defined at the beginning and thus the resulting threshold g_A's are not comparable for different gain distribution profiles. Moreover, experimentalists are more interested in quantities that can be observed or measured in practice. Assuming the net gain is locally proportional to the pump intensity, we may well define an extensive quantity $pump\ level = \int_0^\infty g(x)\cdot x\cdot dx$. As a result, the pump level is related to g_A for different pumping profiles shown in Fig. 2:

(a) Uniform: $g(x) = g_A,\ 0 \le x \le x_b,\ \ pump\ level = \int_0^{x_b} g_A\cdot x\cdot dx = \frac{1}{2} g_A x_b^2$,

(b) Gaussian: $g(x) = g_A \exp\left(-\frac{x^2}{w_p^2}\right),\ x \ge 0,\ \ pump\ level = \int_0^\infty g_A \exp\left(-\frac{x^2}{w_p^2}\right)\cdot x\cdot dx = \frac{1}{2} g_A w_p^2$,

#103822 - $15.00 USD Received 7 Nov 2008; revised 18 Dec 2008; accepted 18 Dec 2008; published 22 Dec 2008

(c) Annular: $g(x) = g_A\left[\exp\left(-\frac{(x-x_p)^2}{w_p^2}\right)+\exp\left(-\frac{(x+x_p)^2}{w_p^2}\right)\right],\ x \geq 0,$

$$pump\ level = \int_0^\infty g_A\left[\exp\left(-\frac{(x-x_p)^2}{w_p^2}\right)+\exp\left(-\frac{(x+x_p)^2}{w_p^2}\right)\right]\cdot x\cdot dx$$

$$= g_A\left[w_p^2\exp\left(-\frac{x_p^2}{w_p^2}\right)+\sqrt{\pi}w_p x_p\ \mathrm{erf}\left(\frac{x_p}{w_p}\right)\right],\quad \text{where the error function } \mathrm{erf}(x)\equiv\frac{2}{\sqrt{\pi}}\int_0^x e^{-t^2}dt.$$

3. Numerical results and discussions

3.1. Nonuniform pumping

To be consistent with Part I of this series of papers [3], we still take the coupling coefficients h_1=0.0072+0.0108i and h_2=0.0601 of a quarter-duty-cycle Hankel-phased circular grating the structure of which is described in a previous work [12]. For all the circular DFB, disk-, and ring- Bragg resonator lasers, we assume a typical device size with an exterior boundary radius ρ_b=17.5μm ($x_b=\beta\rho_b\approx$200). The inner disk radius x_0 of the disk Bragg resonator laser is set to be x_b/2=100. The annular defect of the ring Bragg resonator laser is assumed to be located at the middle x_b/2 with its width being a wavelength of the cylindrical waves therein, so that $x_L+x_R=x_b$=200, $x_R-x_L=2\pi$. The parameter w_p in the Gaussian pumping profile is assumed to be x_b/2=100, while the parameters used in the annular pumping profile are $x_p=x_b$/2=100 and $w_p=x_b$/4=50. Introducing all these parameters into Eqs. (1), integrating the equations by Matlab ODE solvers, and then picking up the points satisfying the boundary conditions lead us to the modes of the circular DFB, disk-, and ring- Bragg resonator lasers with their threshold pump levels P_{th} and detuning factors δ under different pumping profiles plotted in Fig. 3. Comparison of the numerically solved modal threshold gains (g_A) with previous analytically solved values [3] in the uniform pumping case concludes that the relative error in the numerical mode solving is within 1%.

Some observations and conclusions are listed as follows: **1.** The modal fields and detuning factors δ are almost unaffected by different pumping profiles since these are inherent properties for a given laser structure; **2.** Gaussian pumping results in the lowest threshold pump levels except for the fundamental (defect) mode of ring Bragg resonator laser; **3.** Annular pumping provides larger threshold discrimination between the fundamental (Mode 1) and first-order (Mode 2) modes of circular DFB and ring Bragg resonator lasers, which is favorable for single-mode operation in these lasers; **4.** Disk Bragg resonator laser still possesses the lowest threshold pump levels among the three types of circular grating lasers [3], while more impressively, Gaussian pumping for this type of laser is much more effective in reducing the threshold pump levels, making them ~3 times lower than those by uniform and annular pumpings.

The above conclusions **2**−**4** can be understood with fundamental laser physics. In any laser structure the overlap factor between the gain spatial distribution and that of the modal intensity is crucial and proportionate. In semiconductor lasers once the pump power is strong enough to induce the population inversion the medium starts to amplify light. The lasing threshold is determined by equating the modal loss with the modal gain, which is the exponential gain constant experienced by the laser mode. This modal gain is proportional to the overlap integral between the spatial distribution of the gain and that of the modal intensity. Therefore if one assumes that, to the first order, the gain is proportional to the excess pump power over the transparency, then the threshold pump level is inversely proportional to the above overlap integral (see, e.g., Sec. 11.3 of [14]). This is just a reflection of the fact that the rate of simulated emission per electron and thus the gain are proportional to the modal intensity as seen by the electron (see, e.g., Sec. 8.3 of [14]). Since the threshold pump levels also depend on specific choice of the pump shape parameters, such as w_p and x_p, the choice of the parameters for a given laser structure should be made such that the pump overlaps with the fundamental mode as much as possible and with the higher-order modes as little as possible. The parameters used in this work are not optimized but representative of decent choices.

#103822 - $15.00 USD Received 7 Nov 2008; revised 18 Dec 2008; accepted 18 Dec 2008; published 22 Dec 2008

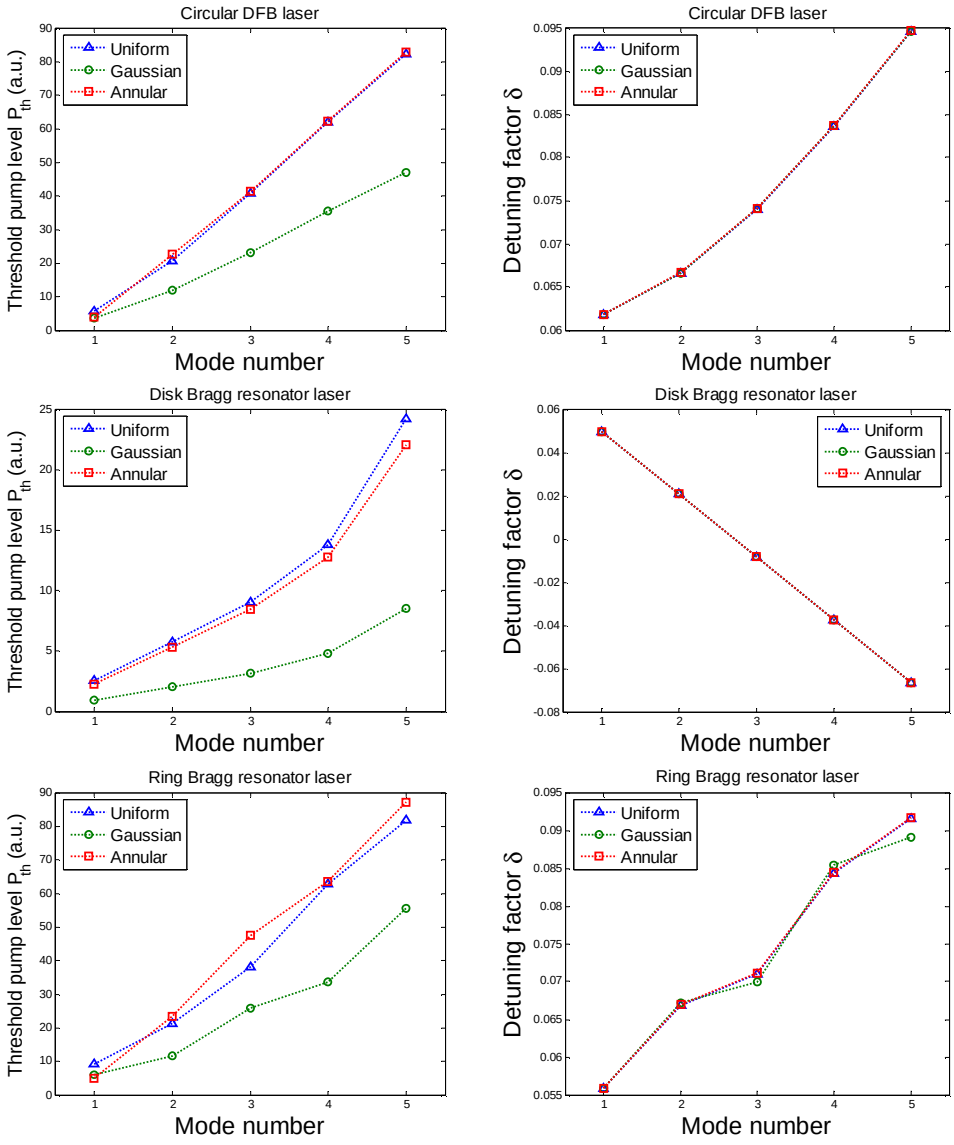

Fig. 3. Threshold pump level P_{th} and detuning factor δ of circular DFB, disk-, and ring- Bragg resonator lasers under uniform, Gaussian and annular pumping profiles.

3.2. Far-field patterns

In the grating regions, the vertical radiation field is related to the in-plane field by Green's function method $\Delta E = \left(s_1 A e^{-i\delta x} + s_{-1} B e^{i\delta x}\right)\left|H_0^{(1)}\right|$ where s_1 and s_{-1} are calculated to be $0.1725-0.0969i$ at the surface [12]. Using the Huygens–Fresnel principle, the diffracted far-field radiation pattern of a circular aperture can be calculated under the parallel ray approximation ($|\mathbf{r}| \gg |\mathbf{r}'|$) [15]:

#103822 - $15.00 USD Received 7 Nov 2008; revised 18 Dec 2008; accepted 18 Dec 2008; published 22 Dec 2008

$$U(\mathbf{r}) \propto \iint_{aperture} \Delta E(\rho,\psi) \frac{\exp\left(ik\left|\mathbf{r}-\mathbf{r}'\right|\right)}{4\pi\left|\mathbf{r}-\mathbf{r}'\right|} d\mathbf{r}' \approx \frac{e^{ikr}}{4\pi r} \iint_{aperture} \Delta E(\rho,\psi) \exp\left(-ik(\mathbf{r}'\cdot\hat{\mathbf{r}})\right) d\mathbf{r}'$$
$$= \frac{e^{ikr}}{4\pi r} \int_{\psi=0}^{2\pi} \int_{\rho=0}^{\rho_b} \Delta E(\rho) \exp\left[-ik\rho\sin\theta\cos(\psi-\phi)\right] \rho d\rho d\psi = \frac{e^{ikr}}{2r} \int_0^{\rho_b} \Delta E(\rho) J_0(k\rho\sin\theta) \rho d\rho \quad (2)$$

where $\mathbf{r}' = \rho\cos\psi\hat{\mathbf{x}} + \rho\sin\psi\hat{\mathbf{y}}$ is the source point and $\mathbf{r} = r\sin\theta\cos\phi\hat{\mathbf{x}} + r\sin\theta\sin\phi\hat{\mathbf{y}} + r\cos\theta\hat{\mathbf{z}}$ is the field point. The far-field intensity pattern is then given by $I(\mathbf{r}) = U^*(\mathbf{r})U(\mathbf{r}) = |U(\mathbf{r})|^2$ and plotted in Fig. 4 for the fundamental modes of circular DFB, disk-, and ring- Bragg resonator lasers.

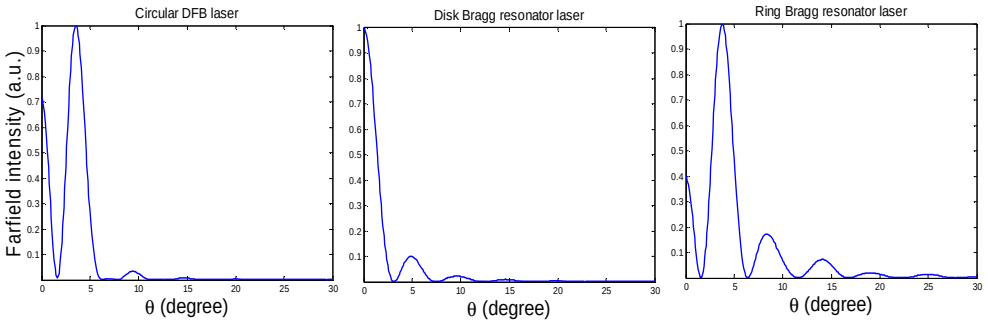

Fig. 4. Far-field intensity patterns of the fundamental modes of circular DFB, disk-, and ring-Bragg resonator lasers.

As expected, the different lobes correspond to different diffraction orders of the light from the circular emission aperture. For circular DFB and ring Bragg resonator lasers, they have most of the energy located in the first-order Fourier component thus their first-order diffraction peaks dominate, while for disk Bragg resonator laser, the zeroth-order peak dominates. These theoretical results are similar to previously published experimental data for circular DFB and DBR lasers [16, 17].

4. Conclusions

Nonuniform pumping and far-field patterns of the surface-emitting chirped-grating circular DFB, disk-, and ring- Bragg resonator lasers have been studied. Their modal properties, especially threshold pump levels and frequency detuning factors, were compared under three pumping profiles − uniform, Gaussian, and annular. A larger overlap between the pumping profile and modal intensity distribution leads to a lower threshold pump level. The comparison concluded that Gaussian pumping results in the lowest threshold pump levels except for the fundamental mode of ring Bragg resonator laser, and annular pumping provides larger threshold discrimination between the fundamental and first-order modes of circular DFB and ring Bragg resonator lasers, which is favorable for single-mode operation in these lasers. The far-field patterns of the fundamental modes of circular DFB, disk-, and ring- Bragg resonator lasers were also acquired and analyzed. It was found that circular DFB and ring Bragg resonator lasers have the first-order dominating peak, while disk Bragg resonator laser has the zeroth-order dominating peak.

Acknowledgments

This work was supported in part by the Defense Advanced Research Projects Agency (DARPA) and in part by the National Science Foundation. X. Sun is grateful to Dr. P. Chak for his kind help in numerical calculations.

#103822 - $15.00 USD Received 7 Nov 2008; revised 18 Dec 2008; accepted 18 Dec 2008; published 22 Dec 2008